Inorganic Chemistry

Article

pubs.acs.org/IC

Corrole and Corrole Functionalized Silica Nanoparticles as New Metal Ion Chemosensors: A Case of Silver Satellite Nanoparticles Formation

Carla I. M. Santos,[†,‡] Elisabete Oliveira,*[,‡,§] Javier Fernández-Lodeiro,[‡] Joana F. B. Barata,[†,∥] Sérgio M. Santos,[∥] M. Amparo F. Faustino,[†] José A. S. Cavaleiro,[†] M. Graça P. M. S. Neves,*[,†] and Carlos Lodeiro*[,‡]

[†]Chemistry Department and QOPNA and [∥]Chemistry Department and CICECO, University of Aveiro, Campus Universitário de Santiago, 3810-193 Aveiro, Portugal

[‡]BIOSCOPE Group, REQUIMTE-CQFB, Chemistry Department, Faculty of Science and Technology, University NOVA of Lisbon, 2829-516 Monte de Caparica, Portugal

[§]Veterinary Science Department, CECAV, University of Trás-os-Montes and Alto Douro, 5001-801 Vila Real, Portugal

Supporting Information

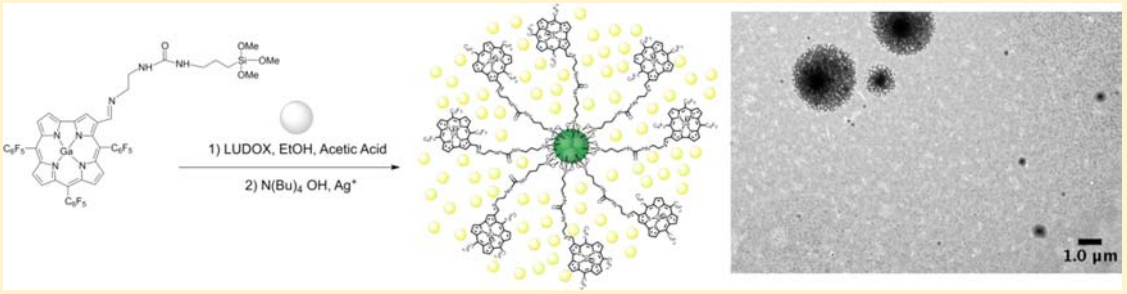

ABSTRACT: Corrole macrocycles are very appealing dyes for incorporation into light harvesting devices. This work shows the sensorial ability of 5,10,15-tris(pentafluorophenyl)corrole **1** and its monoanionic species toward Na^+, Ca^{2+}, Cu^{2+}, Cd^{2+}, Pb^{2+}, Hg^{2+}, Ag^+, and Al^{3+} metal ions in toluene and acetonitrile. The photophysical studies toward metal ions were carried out by absorption and emission spectroscopy. From all metal ions studied, corrole **1** shows to be colorimetric for Hg^{2+} allowing a naked-eye detection of Hg^{2+} through a change of color from purple to blue in acetonitrile and from green to yellow in toluene. In addition a new β-imine corrole **4** was successful synthesized and further functionalized with 3-isocyanatopropyl-trimethoxysilane resulting in an alkoxysilane derivative **5**. The grafting of alkoxysilane derivative **5** with optically transparent silica nanoparticles (SiNPs) was achieved succesfully. The new-coated silica nanoparticles with corrole **5** were studied in the presence of Cu^{2+}, Hg^{2+}, and Ag^+ as metal ion probes. Interestingly, upon addition of Ag^+, groups of satellite AgNPs were formed around the SiNPs and were checked by transmission electron microscopy (TEM). At same time, a change of color from green to yellow was observed.

INTRODUCTION

The design, synthesis, and application of fluorescent molecular probes that selectively recognize the presence of biologically important analytes, such as metal ions, is an area in constant growth.[1] In the past few years the easy detection and quantification of pollutant metallic species by fluorescent molecular probes have attracted interest in fields such as waste management, environmental chemistry, and clinical toxicology.[2]

Corroles are tetrapyrrolic macrocycles with one *meso* carbon less than porphyrin analogues, providing a trianionic coordination sphere that is able to stabilize metal ions in high valent oxidation state.[3] Considering the synthetic approaches developed for corroles, their chemical functionalization can afford new compounds with potential applications as catalysts, dyes for solar energy conversion and in Medicine.[4,5]

These macrocyles also have useful properties to be used as fluorescent probes for molecular recognition.[6] They absorb and emit light in the visible region, and show high excitation coefficients, fluorescent quantum yields, and photostability. Corroles also display inner nitrogen donor atoms available for metal recognition.[7] However, in contrast to porphyrins, the sensorial ability of corroles has been under study. Up to date there are few reports about the use of corroles as sensing materials in analytical chemistry.[8,9]

5,10,15-tris(pentafluorophenyl)corrole **1** is one of the most studied macrocycles of the corrole family, and one of our major interests is concerned with its functionalization and further applications.[10]

Among the metal ions, we are particularly interested in metals with biological and environmental impact.[1,6,11−17]

In this way we decided to evaluate the sensorial ability of 5,10,15-tris(pentafluorophenyl)corrole **1** in the absence and in

Received: March 14, 2013
Published: July 15, 2013

 © 2013 American Chemical Society dx.doi.org/10.1021/ic4006295 | *Inorg. Chem.* 2013, 52, 8564−8572

the presence of OH^- anion toward Na^+, Ag^+, Ca^{2+}, Cu^{2+}, Cd^{2+}, Pb^{2+}, Hg^{2+}, Ni^{2+}, Zn^{2+}, Al^{3+}, Cr^{3+}, Fe^{3+}, and Ga^{3+} metal ions in the aprotic solvents, as toluene and acetonitrile (see Figure 1).

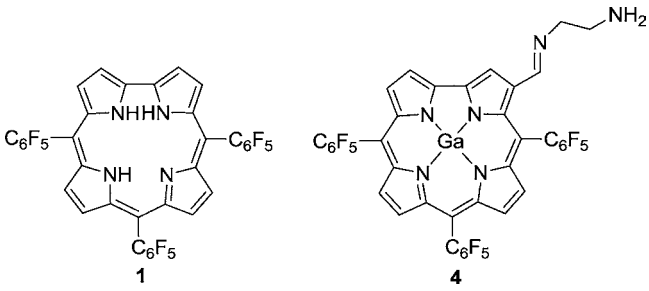

Figure 1. Structure of compounds **1** and **4**.

Taking into account that the incorporation of a highly emissive corrole unit in silica nanoparticles[18] could improve the affinity, versatility, and sensitivity of the chromophore to the guest, we decide to coat silica nanoparticles with corrole **5** via an imine linkage (see Figure 1). The sensorial ability of these nanoparticles was also evaluated toward Hg^{2+}, Ag^+, and Cu^{2+}.

2. EXPERIMENTAL SECTION

2.1. Chemicals and Starting Materials. $AgCH_3SO_3$, $NaCH_3SO_3$, $Ca(CH_3SO_3)_2$, $Cd(CH_3SO_3)_2$, $Cu(BF_4)_2{\cdot}6H_2O$, $Pb(BF_4)_2{\cdot}6H_2O$, $Hg(CH_3SO_3)_2$, $Zn(CH_3SO_3)_2$, $Ni(CH_3SO_3)_2$, $Ga(NO_3)_3{\cdot}xH_2O$, $Cr(NO_3)_3{\cdot}9H_2O$, $FeCl_3{\cdot}6H_2O$, and $Al(NO_3)_3{\cdot}9H_2O$ salts, and $(CH_3)_4NOH$ (tetramethylammonium hydroxide), have been purchased from Strem Chemicals, Sigma Aldrich and TCI. Ethylenediamine, triethylamine, anhydrous sodium sulfate acetic acid and silica gel for thin layer chromatography (TLC) were purchase from Merck. Ludox AS-30 silica nanoparticles by Sigma-Aldrich (30 nm). Water was always used purified and deionized (Milli-Q grade, Millipore).

All chemicals were used without further purification with the exception of triethylamine which was dried under standard procedures. The solvents were obtained from Panreac and Riedel-de-Häen with HPLC grade. Absolute ethanol, dichloromethane, and pentane were distilled and dried under standard procedures.

2.2. Spectrophotometric and Spectrofluorimetric Measurements. Absorption spectra were recorded on a JASCO V-650 spectrophotometer and the fluorescence emission on a spectrofluorimeter HORIBA-JY Scientific Fluoromax-4. The linearity of the fluorescence emission vs the concentration was checked out in the concentration used (10^{-4}–10^{-6} M). A correction for the absorbed light was performed when necessary. The spectrometric characterizations and titrations were performed as follows: the stock solutions of compounds **1** and **4** (ca. 10^{-3} M) were prepared by dissolving an appropriate amount of each compound in a 10 mL volumetric flask and diluting it to the mark with toluene or acetonitrile. The solutions were prepared by appropriate dilution of the stock solutions up to 10^{-5}–10^{-6} M. Titrations of compounds **1** and **4** were carried out by adding microliter amounts of standard solutions of the ions in DMSO or acetonitrile, when the ligand was in toluene or acetonitrile, respectively. All studies have been performed in standard quartz cells with 1 cm pathway.

The spectrometric characterization of silica nanoparticles functionalized with corrole **5** was performed in dichloromethane. Titrations involving silica nanoparticles were carried out by the addition of microliter amounts of solutions of metals in dimethylsulfoxide (DMSO) or acetonitrile. All the luminescence measurements were performed at 298 K.

Fluorescence quantum yield of compound **4** was measured using a solution of cresyl violet perchlorate in absolute ethanol as a standard ($[\phi]$ = 0.54)[19] and was corrected for different refraction indexes of solvents. The limit of detection (LOD) and the limit of quantification (LOQ) for the metal ions were performed, having in mind their use for real metal ion detection and for analytical applications. For these measurements, ten different analyses for the selected receptor were performed to obtain the LOQ. The LOD was obtained by applying the formula:

$$y_{dl} = y_{blank} + 3\text{std}$$

where y_{dl} = signal detection limit and std = standard deviation.

2.3. TEM Measurements. To obtain the transmission electron microscopy (TEM) images of the samples, 1 μL of the colloidal suspension was dropped on a copper grid coated with a continuous carbon film, and the solvent was allowed to evaporate. TEM images were obtained through a JEOL JEM 1010F transmission electron microscope operating at 100 kV. Data for size distribution histograms were made by measuring for the smaller nanoparticles in more than 200 particles per sample in several TEM images.[20]

2.4. Spectroscopic Characterization of Ligands. ^{1}H NMR and ^{19}F NMR spectra were recorded on Bruker Avance 300 (at 300 and 282 MHz, respectively) spectrometer. $CDCl_3$ and pyridine-d_5 were used as solvents with tetramethylsilane (TMS) as the internal reference; the chemical shifts are expressed in δ (ppm) and the coupling constants (J) in hertz (Hz).

High-resolution mass spectra analysis (HRMS-ESI$^+$) was performed on a microTOF (focus) mass spectrometer. Ions were generated using an Apollo II (ESI) source. Ionization was achieved by electrospray, using a voltage of 4500 V applied to the needle, and a counter voltage between 100 and 150 V applied to the capillary.

IR spectra were obtained for KBr pellets, in the range 400–4000 cm^{-1}, with a Shimadzu FTIR 8400S instrument.

2.5. Synthesis of Ligands. The 5,10,15-tris(pentafluorophenyl)-corrole **1** was synthesized by condensation of pentafluorobenzaldehyde with pyrrole at room temperature, according to the literature,[21] and the 5,10,15-tris(pentafluorophenyl)corrolatogallium(III)-(pyridine) **2** was obtained by refluxing the free base **1** in pyridine with $GaCl_3$.[22] The gallium complex of 5,10,15-tris(pentafluorophenyl)-corrole-3-carbaldehyde **3** was obtained by Vilsmeier–Haack formylation of corrole **2** using $POCl_3$ and DMF.[23]

*2.5.1. Synthesis of 3-(2-Aminoethyl)imino)methyl)-5,10,15-tris-(pentafluorophenyl)corrolate Gallium(III) **4**.* Ethylenediamine (3.4 mg, 0.056 mmol) was added to a solution of **3** (25 mg, 0.028 mmol) in ethanol absolute (5 mL). The resulting solution was gently refluxed with magnetic stirring for about 4 h. After this period, the solvent was evaporated under reduced pressure, and the resultant product crystallized from a mixture of dichloromethane–hexane (18.2 mg, 69% yield).

^{1}H NMR (300.13 Hz, $CDCl_3$, a few drops of pyridine- d_5): 9.28 (s, 1H, H-2), 9.18 (d, 1H, J 4.1, H-18), 8.80–8.74 (m, 4H, H-β), 8.66 (s, 1H, H-1′), 8.54 (d, 1H, J 4.1, H-17), 4.13 (s, 2H, N–H), 3.25–3.23 (m, 2H,CH_2), 3.01–2.97(m, 2H,CH_2).

^{19}F NMR (282.37, $CDCl_3$, a few drops of pyridine-d_5): δ −185.78 to −185.75 (m; 1 F; F*meta*); −185.62 to −185.59 (m; 1 F; F*meta*); −185.51 to −185.35 (m; 1 F; F*meta*); −185.12 to −185.05 (m; 2 F; F*meta*); −184.98 to −184.96 (m; 1 F; F*meta*); −176. 90 (t; 1 F; J 21.2 Hz; F*para*); −176.59 (t; 1 F; J 21.2 Hz; F*para*); −175,19 (t; 1 F; J 21.2 Hz; F*para*), −163.38 (dd; 1 F; J 24.0 Hz and J 7.1 Hz; F*ortho*); −160. 94 (dd; 1 F; J 25.4 Hz e J 8.5 Hz; F*ortho*), −160.91 to −160.82 (m; 3 F; F*ortho*), −159.16 (dd; 1 F; J 24.0 Hz and J 7. One Hz; F*ortho*).

IR (cm^{-1}): 3484 (N–H, Amine), 1657 (C=N, Imine), 1589 and 1492 (C=C, Ar).

HRMS [ESI$^+$]: m/z ([M+H]$^+$) calcd for $C_{40}H_{14}F_{15}GaN_6$: 933.1352, found: 933.1316 λ_{max} (log ε) CH_2Cl_2 410 (4.61), 432 (5.21), 601 (4.35), 623 (4.48) nm.

*2.5.2. Synthesis of Silane Corrole **5**.* Corrole **4** (16 mg, 0.017 mmol) was dissolved in 5 mL of dichloromethane, followed by the addition of triethylamine (3 μL, 0.017 mmol) and of the linker 3-isocyanatopropyltrimethoxysilane (3.6 mg, 0.017 mmol). The reaction mixture was kept under stirring at room temperature for 2 days. After this period the solvent was evaporated, and the resulting solid was washed under vacuum. Compound **5** was used in the subsequent reaction without further purification (12.6 mg, 64% yield).

dx.doi.org/10.1021/ic4006295 | Inorg. Chem. 2013, 52, 8564–8572

Scheme 1. General Synthetic Pathway of Compounds 4 and 5

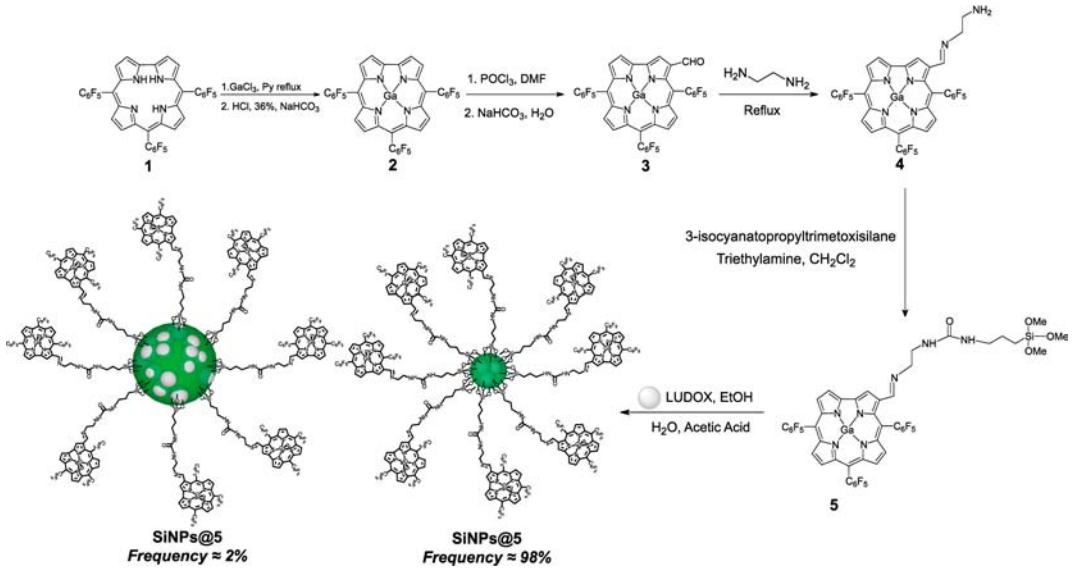

^{1}H NMR (300.13 Hz, $CDCl_3$, a few drops of pyridine- d_5): 9.63 (s, 1H, H-2), 9.10 (d, 1H, *J* 4.0, H-18), 8.76−8.72 (m, 3H, 2H-β + H-1′), 8.67(d, 1H, H-β, *J* 4.9 Hz), 8.51 (d, 1H, H-β, *J* 4.7 Hz), 8.47 (d, 1H, H-β, J 4.5 Hz), 5.52 (bs, 1H, NH) 5.04 (bs, 1H, NH), 3.84−3.74 (3×CH_3 under solvent), 3.28−3.30 (m, 4H, 2× CH_2), 3.17−3.12 (m, 2H, CH_2), 1.63−1.60 (m, 2H, CH_2), 0.65−0.60 (m, 2H, CH_2).

HRMS [ESI$^+$]: $[M+H]^+$ calcd for $C_{47}H_{29}F_{15}GaN_7O_4Si$: *m*/*z* 1138.1048, found: *m*/*z* 1138.1036.

Elem Anal. Calc. for $C_{47}H_{29}F_{15}GaN_7O_4Si$. 2 CH_2Cl_2. 2 C_5H_{12}: C, 48.78; H, 3.95; N, 6.75. Found: C, 48.43; H, 3.81; N, 6.46.

λ_{max} (log ε) CH_2Cl_2 413 (4.53), 436 (5.25), 603 (4.31), 626 (4.47) nm.

2.5.3. Synthesis of Silica Nanoparticles Decorated with Compound 5. Compound **5** (12 mg, 0.011 mmol) was dissolved in a mixture of 0.5 mL of ethanol, 0.5 mL of water, 0.5 mL of CH_3COOH, and 0.680 mL of a water solution of commercial Ludox AS-30 silica nanoparticles (30 nm). The resultant mixture was stirred at 80 °C for 2 days, then 200 μL were withdrawn, dissolved in 1 mL of dichloromethane, and centrifuged at 6000 rpm, at 21 °C, for 10 min. The pellet was washed three times with ethanol (3 × 1 mL), and finally dissolved in 0.5 mL of dichloromethane.

The commercial silica nanoparticles (LUDOX) were measured by TEM and dynamic light scattering (DLS), and a diameter of 30 ± 5 nm (TEM) and a hydrodynamic diameter of 40 ± 3 nm (DLS) were determined, respectively. TEM measurements of the new material SiNPs@**5** revealed a diameter of 80 ± 30 nm in 98%. A smaller population of bigger nanoparticles about 2% was observed with 600 ± 200 nm.

UV−vis absorption band (dichloromethane) = 601 nm; emission band (dichloromethane) = 624 nm; fluorescent quantum yield = 0.03.

3. RESULTS AND DISCUSSION

3.1. Synthesis. The synthetic route used to prepare the precursor **5** for further coating with commercial silica nanoparticles is outlined in Scheme 1. The 5,10,15-tris-(pentafluorophenyl)corrole **1**,[21] the corresponding gallium-(III)(pyridine) complex **2**[22] and the gallium(III) complex of 5,10,15-tris(pentafluorophenyl)corrole-3-carbaldehyde **3** were synthesized according to the procedures described previously.[23]

The protection of the corrole **1** with gallium(III) was fundamental to obtain efficiently the 5,10,15-tris-(pentafluorophenyl)corrole-3-carbaldehyde **3** under Vilsmeier−Haack conditions.

The synthesis of the new β- imine corrole **4** was carried out by adding ethylenediamine to an absolute ethanol solution of β-formyl corrole **3**. The reaction was performed at reflux, for 4 h. The TLC control revealed the absence of the starting corrole **3** and the presence of a new product. After workup, this compound was identified by NMR and HRMS as the novel corrole derivative **4**, obtained in 69% yield. The ^{1}H NMR spectrum showed at lower field, a singlet at δ 9.28 corresponding to the resonance of β-pyrrolic H-2 and a doublet at δ 9.18 due to the resonance of proton H-18. Besides the resonances of the β-pyrrolic protons H-17 (δ 8.54 doublet) and H-7,8,12,13 (δ 8.80−8.74 multiplets), the ^{1}H NMR spectrum showed a singlet at δ 8.66 identified as the resonance of proton H-1′, and a broad signal at δ 4.13 as the resonance of the NH_2 protons. In the aliphatic region, the spectrum presented two multiplets between δ 3.25 and δ 3.23 and δ 3.01 and δ 2.97 corresponding to the resonances of the protons of the ethyl group.

The functionalization reaction of the imine-corrole **4** with 3-isocyanatopropyl-trimethoxysilane was performed in dichloromethane in the presence of triethylamine. The success of the coupling was confirmed by HRMS; the mass spectrum of intermediate **5** showed the expected molecular ion $[M + H]^+$ at *m*/*z* 1138.1036. The grafting of alkoxysilane derivative **5** with LUDOX was achieved by magnetic stirring, at 80 °C for two days. The resulting nanoparticles were further characterized by UV−vis, fluorescence emission spectroscopy, and TEM.

3.2. Spectrophotometric and Spectrofluorimetric Titrations and Metal Ion Sensing Effects in the Presence of Corrole 1. To further understand how 5,10,15-tris-(pentafluorophenyl)corrole **1**, the corrole precursor, behaves in the presence of cations, its sensorial ability was evaluated.

The first studies concerning the sensorial ability of compound **1** toward the different metals, Ag^+, Na^+, Ca^{2+} Cd^{2+}, Pb^{2+}, Zn^{2+}, Ni^{2+},Cu^{2+}, Hg^{2+}, Fe^{3+}, Cr^{3+}, Ga^{3+}, Al^{3+}, were performed in toluene, where the decomposition of the corrole macrocycle is minimized.[24]

The absorption spectrum of compound **1** in toluene shows the Soret-type band at 415 nm and the Q-type band centered at 565 nm, while the emission spectrum shows a band at 645 nm, with a fluorescence quantum yield of 0.05.[9] To avoid the

dx.doi.org/10.1021/ic4006295 | Inorg. Chem. 2013, 52, 8564−8572

reabsorption phenomena, the emission spectrum was collected on the Q-bands. However, no significant changes were detected in the ground and excited state of this corrole after titration in the presence of the metals selected.

Knowing that compound **1** presents a high N−H acidity being really sensitive to anions prompts us to evaluate if its metal sensing ability is modified after deprotonation with OH^-.[25]

The addition of this anion to corrole **1** promotes in the absorption spectrum a decrease accompanied by a red shift in the Soret band from 415 to 440 nm ($\Delta\lambda$ = 25 nm) and in the Q-band from 565 to 606 nm ($\Delta\lambda$ = 41 nm) (see Figure 2). At

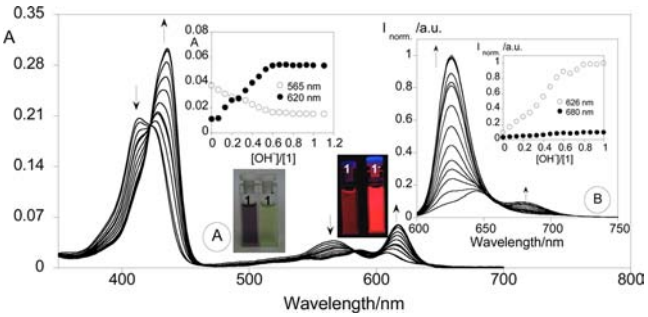

Figure 2. Spectrophotometric (A) and spectrofluorimetric (B) titration of compound **1** with the addition of OH^- in toluene. The inset represents the absorption (A) and the emission intensity (B) as a function of $[OH^-]/[\mathbf{1}]$ at 415 nm, 440 nm, 565 nm, and 620 nm for (A), 626 and 680 nm for (B). ($[\mathbf{1}] = 1 \times 10^{-5}$ M, λ_{exc} = 565 nm, T = 298 K).

same time, a naked-eye change of color from purple to green is visualized upon addition of OH^-. In the fluorescence spectra a strong enhancement in the emission intensity at 644 nm was observed, as well as a blue shift from 644 to 626 nm (see Figure 2 and picture in Figure 2). In addition in the emission spectra the appearance of a new band was detected at 670 nm. These features are similar to the ones described for corroles in the presence of organic bases,[26] confirming that after titration we are in the presence of the monoanionic form of a corrole $[(Cor)H_2]^-$. A similar spectroscopic profile was also reported by Gross and co-workers,[25] where a pH study was carried out, allowing to conclude that the pH range at which neutral corroles exist is extremely limited.

Corrole **1** does not present any spectral changes in the ground and excited states after addition of the metal ions mentioned above.

However, the addition of Cu^{2+}, Cd^{2+}, Pb^{2+}, Hg^{2+}, Ga^{3+}, Cr^{3+}, Fe^{3+}, Ag^+, or Al^{3+} to compound **1**, after its previous deprotonation with 0.5 equiv of OH^-, is responsible for significant alterations in the absorption and emission spectra. Only the titrations with Na^+, Ca^{2+}, Ni^{2+}, Zn^{2+} did not affect the ground and the excited state of the monoanionic form of corrole **1** that will be referred here as $\mathbf{1}^-$.

Figure 3 shows the modifications observed in the absorption and emission spectra of $\mathbf{1}^-$ in the presence of Cd^{2+}, Cu^{2+} and in Figure 4 in the presence of Hg^{2+}. The titrations including the other metal ions (Ga^{3+}, Fe^{3+}, Cr^{3+}, Pb^{2+}, Al^{3+}, and Ag^+), since they presented similar behavior, are shown in the Supporting Information, Figures SN1 and SN2. The addition of Cd^{2+} produces alterations in the absorption spectrum, such as, a decrease in the Q-type absorption band at 620 nm and in the Soret-type band at 440 nm that is accompanied with the

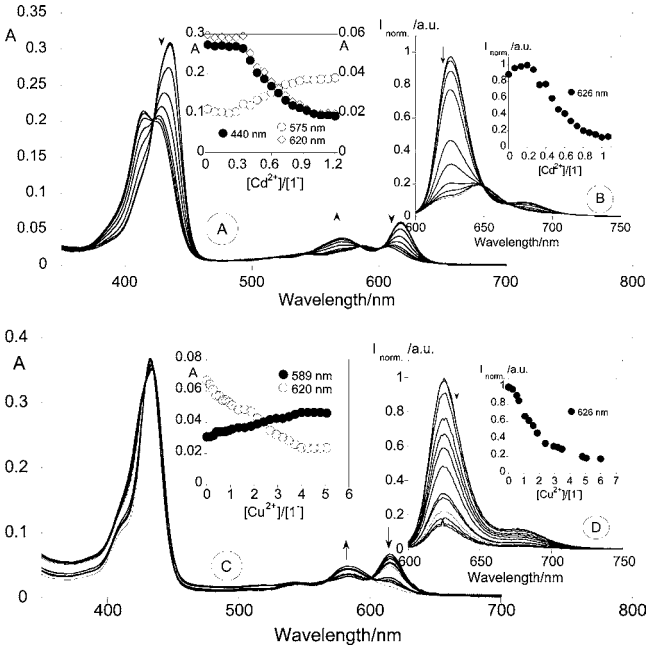

Figure 3. Spectrophotometric (A, C) and spectrofluorimetric (B, D) titration of $\mathbf{1}^-$ with the addition of Cd^{2+} (A, B) and Cu^{2+} (C, D) in toluene. The inset represents the absorption at 440 nm, 575 nm, and 620 nm for A, at 589 and 620 nm for C; and the emission intensity at 626 nm (B, D) as a function of $[Cd^{2+}]/[\mathbf{1}^-]$, and $[Cu^{2+}]/[\mathbf{1}^-]$, respectively. ($[\mathbf{1}^-] = 1 \times 10^{-5}$ M for $[Cd^{2+}]$ and $[\mathbf{1}^-] = 1.2 \times 10^{-5}$ M for $[Cu^{2+}]$, λ_{exc} = 565 nm, T = 298 K).

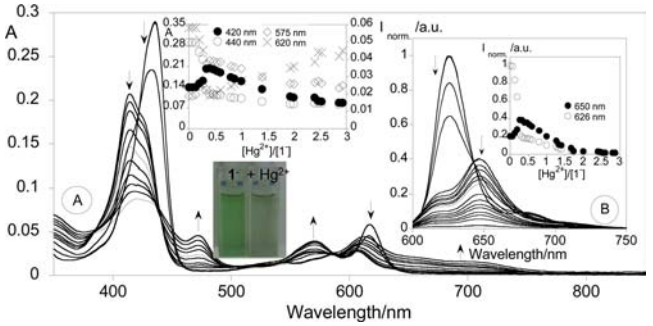

Figure 4. Spectrophotometric (A) and spectrofluorimetric (B) titration of compound $\mathbf{1}^-$ with the addition of Hg^{2+} in toluene. The inset represents the absorption (A) and the emission intensity (B) as a function of $[Hg^{2+}]/[\mathbf{1}^-]$ at 420 nm, 440 nm, 575 nm, and 620 nm for (A), and 626 and 650 nm for (B). ($[\mathbf{1}^-] = 9.0 \times 10^{-6}$ M, λ_{exc} = 565 nm, T = 298 K).

concomitant appearance of blue-shifted bands at 606 nm ($\Delta\lambda$ = 14 nm) and at 415 nm ($\Delta\lambda$ = 25 nm). An isosbestic point at 426 nm was observed.

Considering the fluorescence spectra, the addition of these metal ions promotes a quenching in the emission intensity at 626 nm, accompanied by a red shift from 626 to 645 nm ($\Delta\lambda$ = 19 nm).

The titration with Cu^{2+} produces only alterations in the Q-band region in the absorption spectra where a decrease of the band at 620 nm with the concomitant appearance of a blue shift band at 589 nm is observed. In the emission spectra a quenching was only observed in the emission intensity at 626 nm without any shift (Figure 3D).

The most interesting results arise from the interaction of the monoanionic form of corrole **1** with Hg^{2+}, where a colorimetric

dx.doi.org/10.1021/ic4006295 | Inorg. Chem. 2013, 52, 8564−8572

effect was visualized, with a change of color from dark *green* to *pale* green (see Figure 4). The addition of Hg^{2+} to $\mathbf{1}^-$ results in a blue shift of the Soret band from 440 to 420 nm ($\Delta\lambda$ = 20 nm) and in the Q-type band from 620 to 575 nm ($\Delta\lambda$ = 45 nm) with a decrease in the absorbance. The appearance of a charge transfer band (LMCT, ligand to metal charge transfer) at 478 nm and at 720 nm was observed as well. The blue shift in the ICT (intramolecular charge transfer) transitions can be attributed to Hg^{2+} metal ion binding to free nitrogen atoms in the inner of the macrocycle. In the emission spectra, the addition of Hg^{2+} is responsible for the total quenching in the fluorescence intensity at 626 nm accompanied by a red shift from 626 to 650 nm. This behavior is not unexpected because of the Hg^{2+} "heavy" metal ion nature, which increases the probability for nonradiative deactivation processes to occur, such as intersystem crossing, responsible for chelation enhancement of quenching (CHEQ) in the emission intensity.[27]

The association constants for the interaction of compound $\mathbf{1}^-$ with the different metal ions were calculated using the HypSpec[28] program and are summarized in Table 1. Using the

Table 1. Association Constants (Emission Data), Detection (LOD), and Quantification (LOQ) Limits of $\mathbf{1}^-$ in Toluene

metal	Log K_{assoc} (L:M)	LOD (ppm)	LOQ (ppm)
Al^{3+}	14.32 ± 0.25 (2:1)	0.03	0.06
Cd^{2+}	10.99 ± 0.01 (2:1)	0.04	0.08
Pb^{2+}	11.32 ± 0.01 (2:1)	0.04	0.07
Hg^{2+}	8.43 ± 0.02 (2:1)	0.02	0.03
Ag^{+}	12.33 ± 0.07 (2:1)	0.02	0.03
Cr^{3+}	12.61 ± 0.02 (2:1)	0.09	0.12
Fe^{3+}	7.66 ± 0.02 (1:1)	0.04	0.08
Ga^{3+}	6.49 ± 0.02 (1:1)	0.02	0.04
Cu^{2+}	4.23 ± 0.02 (1:1)	0.03	0.06

Job's plot method (see Supporting Information, Figure SN3),[29] the stoichiometry of two ligands per metal ion (L_2M) could be postulated for Cd^{2+}, Pb^{2+}, Ag^{+}, Cr^{3+}, or Al^{3+} and one ligand per metal in the presence of Cu^{2+}, Ga^{3+}, and Fe^{3+}; these results are in accordance with the ones obtained from the HypSpec program.

Looking at Table 1 the most stable complexes were formed with Al^{3+}, Cr^{3+}, and Ag^{+}, with log K_{assoc} = 14.30 ± 0.25, log K_{assoc} = 12.61 ± 0.02, and log K_{assoc} = 12.33 ± 0.07, respectively. From the other association constant values: log $K_{assoc\ Pb}{}^{2+}$ = 11.32 ± 0.01 (L_2M) > log $K_{assoc\ Cd}{}^{2+}$ = 10.99 ± 0.01 (L_2M) > log $K_{assoc\ Hg}{}^{2+}$ 8.43 ± 0.02 (L_2M) > log $K_{assoc\ Fe}{}^{3+}$ 7.66 ± 0.02 (LM) > log $K_{assoc\ Ga}{}^{3+}$ 6.49 ± 0.02 (LM) > log $K_{assoc\ Cu}{}^{2+}$ = 4.23 ± 0.02 (LM) we can conclude that the monoanion of corrole **1** coordinated better with Pb^{2+} followed by Cd^{2+}, Hg^{2+}, and finally Cu^{2+} metal ions.

Apart from the type of donor atoms present in the inner of the corrole, where the metal complexation occurs, other parameters in the macrocycle such as the cavity size, shape, conformation, topology, and rigidity and the radius of the metal ion are important because they influence the thermodynamic and kinetics properties of the corresponding final metal complexes. Moreover, in macrocyclic ligands the chelate and macrocycle effects must be taken into account.[30,31]

Figure 5 shows the normalized fluorescence intensity of corrole **1** after being deprotonated with OH^- and after the addition of 0.5 equiv of M^{n+} metal ions in toluene, (M^{n+} = Na^+, Ca^{2+}, Ni^{2+}, Zn^{2+}, Cd^{2+}, Cu^{2+}, Pb^{2+}, Hg^{2+}, Ga^{3+}, Cr^{3+}, Fe^{3+}, Ag^+, and Al^{3+} ions), after deprotonating corrole **1** with OH^- anion.

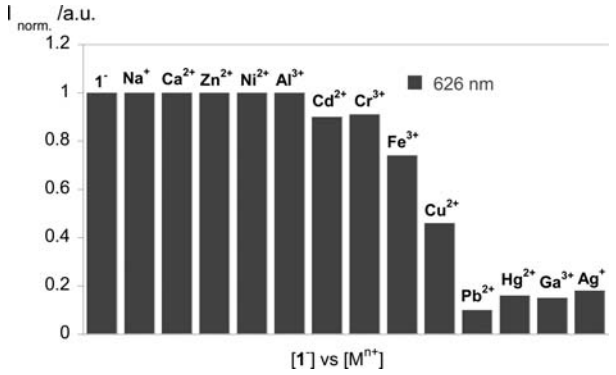

Figure 5. Normalized fluorescence at 626 nm of compound **1** with the first addition of OH^- (species $\mathbf{1}^-$), and after addition of 0.5 equiv of [M^{n+} = Na^+, Ca^{2+}, Ni^{2+}, Zn^{2+}, Cd^{2+}, Cu^{2+}, Pb^{2+}, Hg^{2+}, Ga^{3+}, Cr^{3+}, Fe^{3+}, Ag^+, and Al^{3+}] = M^{n+} metal ions in toluene.

Taking into account the results of Figure 5, we can see the evident CHEQ effect of the specie $\mathbf{1}^-$ in the presence of 0.5 equiv of the heavy pollutants and toxic Pb^{2+}, Hg^{2+}, Cd^{2+}, and Ag^+ metal ions, while a strong quenching between 50% and 80% was observed.

The detection (LOD) and quantification (LOQ) limits for the metal ions studied were also determined in the presence of the monoanionic form $\mathbf{1}^-$, using the emission band centered at 626 nm (Table 1). The values obtained show that the lowest values of LOD and LOQ were found for Ag^+; with this macrocycle the minimum amount of Ag^+ detectable was 0.02, and the minimum amount quantified was 0.03 ppm.

Since all the metal salts used show good solubility in acetonitrile, it was decided to perform several titrations toward the same metal ions, in this solvent with and without the previous addition of OH^- anion. When the titrations were carried after deprotonation with OH^-, no spectral alterations were detected in the absorption and emission spectra. However, without the previous addition of OH^- anion, the increase of the dipole moment of the solvent from 0.36 D (toluene) to 3.92 D (acetonitrile), leaded to a better sensorial and selectivity capability of corrole **1** for Hg^{2+}. In Figure 6 are presented the modifications observed in the absorption and emission spectra of compound **1** with the increasing addition of Hg^{2+} metal ion. In these conditions, no changes were detected in the ground and excited state of corrole **1** upon addition of the other metal ions studied.

In this case, the Soret band of compound **1** upon addition of Hg^{2+} was practically not affected, whereas the Q-band region showed significant changes. Looking at Figure 6A, it can be observed that the addition of the metal ion is responsible by a decrease in the absorbance band at 565 nm that is accompanied by the appearance of two bands at 635 and 680 nm. In these conditions a colorimetric effect (a change of color from purple to green-blue) was also observed, which allows again a naked-eye detection of Hg^{2+} (see Figure 6C). In the emission spectra a quenching was seen in the emission intensity at 645 nm (Figure 6B). The association constant was also determined by use of the HypSpec program, and the value obtained for **1** in the presence of Hg^{2+} (acetonitrile) was log $K_{assoc\ Hg}{}^{2+}$ = 9.04 ± 0.01, with a stoichiometry of two ligands per one metal ion, which is slightly higher than the one obtained for $\mathbf{1}^-$ in the

dx.doi.org/10.1021/ic4006295 | *Inorg. Chem.* 2013, 52, 8564−8572

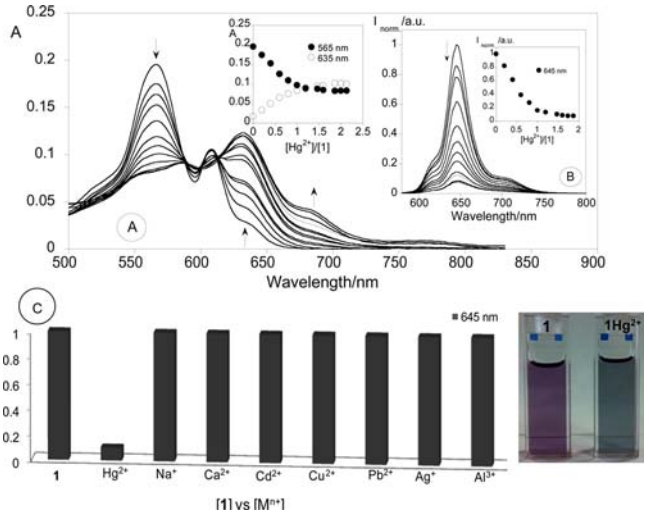

Figure 6. Spectrophotometric (A) and spectrofluorimetric (B) titration of **1** with the addition of Hg^{2+} in acetonitrile. The inset represents the absorption (A) and the emission intensity (B) as a function of $[Hg^{2+}]/[\mathbf{1}]$ at 565 and 635 nm for (A), 645 nm for (B). ($[\mathbf{1}] = 1 \times 10^{-5}$ M, λ_{exc} = 565 nm, T = 298 K). (C) Normalized fluorescence at 645 nm of compound **1** with addition of 0.5 equiv of metal ions in acetonitrile [(Na^+, Ca^{2+}, Cd^{2+}, Cu^{2+}, Pb^{2+}, Hg^{2+}, Ag^+, and Al^{3+}) = M^{n+}]; and picture with a color change from purple to green-blue with the addition Hg^{2+} in acetonitrile.

presence of Hg^{2+} in toluene [log $K_{assoc\ Hg}{}^{2+}$ = 8.43 ± 0.02, (L_2M)].

As a conclusion, corrole **1** in acetonitrile shows a higher affinity and an unprecedented selectivity for Hg^{2+} metal, as can be seen in Figure 6C, where a normalized intensity of fluorescence toward the addition of 0.5 equiv of metal ions studied is shown.

3.2.1. Theoretical Studies. To understand better the complex formation, the preferential stoichiometries and binding modes of corrole $\mathbf{1}^-$ to Al^{3+}, Cu^{2+}, and Ag^+ were assessed through a series of electronic calculations[32] performed at the density functional theory (DFT) level, using Gaussian09.[33] The energetics of the 1:1 and 2:1 (receptor:ligand) binding stoichiometries was evaluated by calculating the energy gain/loss obtained upon formation of the complex from its individual components.

The complexation of Al^{3+} with $\mathbf{1}^-$ occurs preferentially in a 2:1 stoichiometry, as shown in Figure 7. The coordination of the cation occurs with four nitrogens from one corrole unit and with one nitrogen from a second corrole, with $Al^{3+}\cdots N$ distances ranging from 1.91 to 2.12 Å, in what resembles a square pyramid coordination environment. Our DFT calculations revealed that this 2:1 binding arrangement is more stable than the 1:1 stoichiometry in about −0.127 Ha (−332.8 kJ mol^{-1}; see Figure 8 for the analogous 1:1 complex with Cu^{2+}). The lack of stability of the 1:1 complex with Al^{3+} seems to arise from the fact that the cation, to efficiently coordinate with all four nitrogens, needs to fully fit inside the corrole cavity, which then leads to electrostatic repulsion between the cation and the two positively charged interior protons. However, when considering the 1:1 binding arrangement of $\mathbf{1}^-$ with Cu^{2+}, as shown in Figure 7, the larger size of the Cu^{2+} cation requires that coordination occurs slightly above the corrole plane, thus minimizing the electrostatic hindrance between the cation and the interior protons. In this case, the coordination of the cation occurs with the four nitrogens of the corrole and one oxygen from a solvent molecule (in this case DMSO). The incorporation of two solvent molecules was required to provide the necessary stabilization of the overall complex. In fact, when solvent molecules were not incorporated at all, the 2:1 stoichiometry was slightly more stable than the "unsolvated" 1:1 model in about −0.11 Ha (−307.7 kJ mol^{-1}) which suggested that the completion of the coordination sphere of Cu^{2+} requires at least one solvent molecule, whereas the solvated model is more stable than the 2:1 one in about 0.07 Ha (−185.4 kJ mol^{-1}), thus supporting the 1:1 stoichiometry found experimentally. The coordination environment of the cation is a slightly distorted square pyramid involving the four corrole nitrogens and a nitrogen from a solvent molecule, having $Cu^{2+}\cdots X$ (X = $N_{corrole}$ or O_{DMSO}) distances ranging from 2.01 to 2.57 Å. As also shown in Figure 8, a second DMSO molecule is able to establish two simultaneous hydrogen bonds with the two interior corrole protons, with $O_{DMSO}\cdots H_{corrole}$ distances of 1.779 and 1.928 Å. Finally, the coordination of Ag^+ with $\mathbf{1}^-$ (Figure 9) occurs, similarly to Al^{3+}, in a 2:1

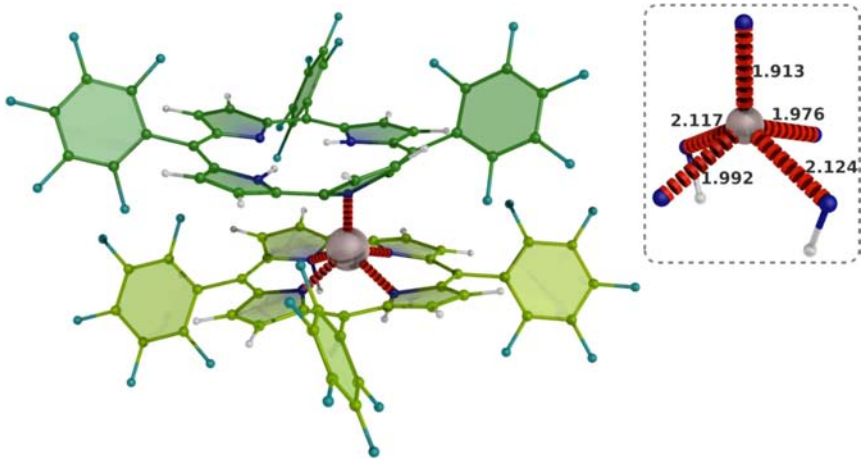

Figure 7. Lowest energy gas-phase complex of $\mathbf{1}^-$ with Al^{3+}, calculated at the B3LYP level. The inset provides details about the coordination environment of the cation, in the same orientation shown for the complex (only key particles were kept for sake of clarity). Coordinating interactions shown as red dashes; distances in Ångstrom. Color code: hydrogen−white; carbon−green (different shades for distinct macrocyles); aluminum−light pink; fluorine−teal, nitrogen−blue.

dx.doi.org/10.1021/ic4006295 | Inorg. Chem. 2013, 52, 8564−8572

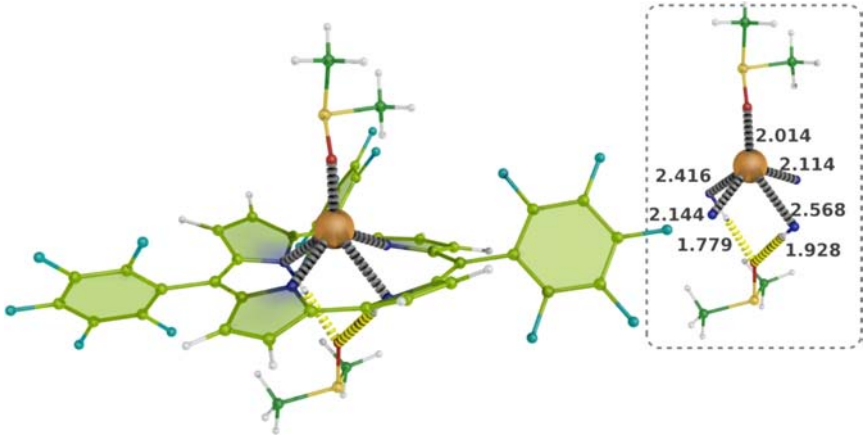

Figure 8. Lowest energy gas-phase complex of $\mathbf{1}^-$ with Cu^{2+}. Details as in Figure 7; Cu^{2+} shown as orange sphere.

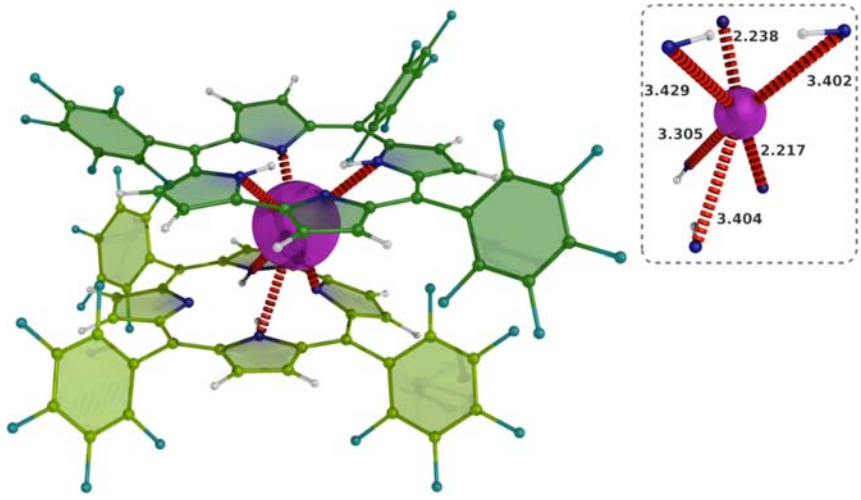

Figure 9. Lowest energy gas-phase complex of $\mathbf{1}^-$ with Ag^+. Details as in Figure 7; Ag^+ cation shown as purple sphere.

stoichiometry, this stoichiometry being more stable than the 1:1 one by about −0.08 Ha (−251.15 kJ mol^{-1}). Coordination of the cation occurs mainly with three nitrogens from one corrole unit and three nitrogens from a second unit, in what resembles a distorted trigonal prismatic coordination environment. The $Ag^+\cdots N$ distances can be subdivided into a set of two shorter distances involving the nonprotonated nitrogens (2.217 and 2.238 Å) and four longer ones involving the protonated nitrogens (ranging from 3.30 to 3.43 Å). Because of the larger cationic radius of Ag^+ relative to that of Al^{3+}, the efficient accommodation of Ag^+ into the binding pocket formed by the two corrole receptors does not impose large distortions on the planarity of the corrolic core, has happens with Al^{3+}.

It is possible that both complexes with Al^{3+} and Ag^+ gain further stabilization in solution from $\pi-\pi$ interactions that can be established as result of the momentary alignment of aromatic fragments from adjacent units. However, evaluation of such hypothesis requires molecular dynamics simulations, which fall beyond the scope of the current analyses.

3.3. Spectrophotometric and Spectrofluorimetric Titrations and Metal Ion Sensing Effects in the Presence of Nanoparticles Functionalized with Silane Derivative 5. To develop new corrole fluorescent materials to be used as new sophisticated metal ion chemosensors in environmental fields, the sensorial ability of the coated silica nanoparticles with compound **5** was studied and compared with that of the free precursor **4**.

The main photophysical data of compound **4** in dichloromethane and in toluene is gathered in Table 2. The Q absorption bands of corrole **4** were centered between 599 and 601 nm, in toluene and CH_2Cl_2, the emission band at 626 and 623 nm, respectively.

The study of the sensorial ability of compound **4** toward metal ions Cu^{2+}, Hg^{2+}, and Ag^+ was carried out by ligand titrations with the addition of small amounts of the adequate metallic salts.

The titrations were followed by UV−vis and fluorescence measurements in toluene. The most significant alterations in

Table 2. Photophysical Data of Corrole 4

		λ_{max} (nm)			Stokes shift (nm)	
compound	solvents	Soret	Q-bands	λ_{em} (nm)	Q-bands	ϕ (sd = 0.01)
4	dichloromethane	432	601	623	22	0.03
	toluene	431	599	624	25	0.03
5	dichloromethane	430	603	626	23	0.03
SiNPs@5	dichloromethane	431	601	624	23	0.03

dx.doi.org/10.1021/ic4006295 | Inorg. Chem. 2013, 52, 8564−8572

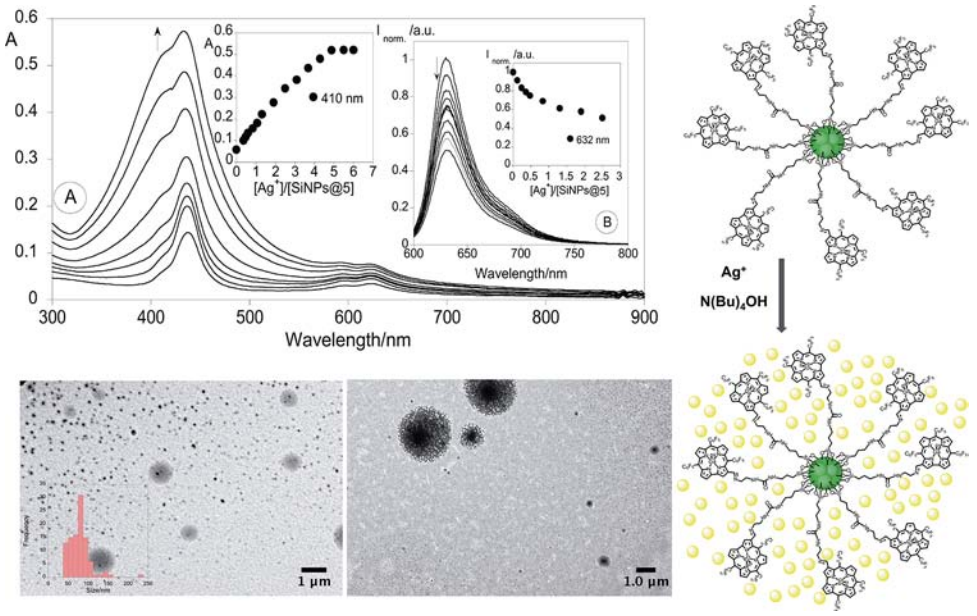

Figure 10. Top: Absorption (A) and emission spectra (B) of SiNPs@**5** with the increasing amount of Ag^+ in dichloromethane; and picture of color change of the nanoparticles' formation. The inset B represents the emission at 626 nm as function of $[Ag^+]/[$ SiNPs@**5**$]$. ($[$SiNPs@**5**$]$ = ca. 5.86×10^{-6} M, λ_{exc} = 410 nm, T = 298 K). **Bottom**: Silica nanoparticles coated with silane derivative **5** (SiNPs@**5**) and with Ag^+ (AgSiNPs@**5**). TEM image of SiNPs@**5** and AgSiNPs@**5**.

the ground and excited states were observed in the presence of the ion Ag^+. No changes were detected in the presence of the ions Hg^{2+} and Cu^{2+}. The addition of Ag^+ to compound **4** promoted a quenching of about 60% at 626 nm in the emission spectrum. Spectral alterations were not observed in the ground state (Supporting Information, Figure SN4).

The profiles of the absorption and emission spectra of the derivatized nanoparticles were very similar to the ones of the ligand **4**. This result is expected since those silica nanoparticles are totally transparent to the visible light and inert to electron-transfer processes.[34] TEM measurements of the new-coated material revealed a diameter of 80 ± 30 nm (98%) demonstrating that the derivatization of Ludox with silane derivative **5** induced nanoparticle growth via aggregation. Moreover, a smaller sample of bigger nanostructures with a 2% of population was observed with sizes of about 600 ± 200 nm. The interaction of the silica nanoparticles coated with the new silane **5** (SiNPs@**5**) was also explored in the presence of Ag^+, Cu^{2+}, and Hg^{2+} metal ions.

The SiNPs@**5** nanoparticles did not show any spectral changes in the presence of Cu^{2+} and Hg^{2+} metal ions, whereas, upon addition of Ag^+ new satellite AgNPs were formed around the silica nanoparticles. Figure 10 shows the silica nanoparticles coated with silane derivative **5** (SiNPs@**5**) and with AgNPs (AgSiNPs@**5**); the TEM images, the spectrophotometric and spectrofluorimetric titrations of SiNPs@**5** with the increasing addition of Ag^+ resulted on the SiNPs@**5** with a layer of AgNPs inducing a strong aggregation.

As can be seen in the absorption spectra of SiNPs@**5**, the increase of Ag^+ amount induced the formation of satellite AgNPs around the silica nanoparticles coated with compound **5**. Its formation is proven by a change of color from green to yellow, as well as by the appearance of a resonance plasmon band centered at 410 nm. Through TEM images it is possible to visualize the formation of the satellite AgNPs around the SiNPs@**5**, affording AgSiNPs@**5** with sizes around 600 ± 200 nm, and a small population between 2 and 5% of bigger nanostructures was detected. These macro nanostructures are due to self-aggregation after interaction with the corrole **5** and silver ions.

The polydispersed distribution of AgSiNPs@**5** can be due to the stepwise addition of Ag^+. The decrease observed in the emission intensity in the fluorescent spectra is probably due to the proximity between silver and the nanoparticle monolayer increasing the accessibility to nonradiative processes.

4. CONCLUSIONS

Corrole **1** was successfully studied in the presence Ag^+, Na^+, Ca^{2+}, Zn^{2+}, Cd^{2+}, Cu^{2+}, Pb^{2+}, Hg^{2+}, Zn^{2+}, Ni^{2+}, Cr^{3+}, Ga^{3+}, Fe^{3+}, and Al^{3+} metal ions in toluene and acetonitrile. Metal complexes with formula L_2M, were obtained in the interaction of $\mathbf{1}^-$ with Cd^{2+}, Pb^{2+}, Hg^{2+}, Ag^+, Cr^{3+}, and Al^{3+}, while LM species were identified with Cu^{2+}, $Ga^{3+,}$ and Fe^{3+}, in toluene. The higher association constants were observed for Ag^+, Cr^{3+}, and Al^{3+}. In toluene, the species corrole $\mathbf{1}^-$ shows to be a naked eye sensor in the presence of Hg^{2+}; a change of color from dark green to green was vizualized. Also, corrole **1** reveals to be selective for Hg^{2+} in acetonitrile, where a change of color from purple to green-blue was observed.

A new sophisticated material based on silica nanoparticles coated with compound **5** was successfully synthesized and studied in the presence Cu^{2+}, Hg^{2+}, and Ag^+ metal ions. Upon addition of Ag^+ new satellite AgNPs were formed around the silica nanoparticles, followed by a change of color from green to yellow.

All these promising results support the use of chemosensor derivatives based on corroles in environmental control, biology, chemistry, or medicine. It is also important to point out the efficiency of species $\mathbf{1}^-$ against the heavy pollutants and toxic Pb^{2+}, Hg^{2+}, and Ag^+ metal ions, whereas a strong and very effective quenching was observed only with the addition of 0.5 equiv of metal ion.

dx.doi.org/10.1021/ic4006295 | Inorg. Chem. 2013, 52, 8564−8572

■ ASSOCIATED CONTENT

Supporting Information

Further details are give in Figures SN1−SN6. This material is available free of charge via the Internet at http://pubs.acs.org.

■ AUTHOR INFORMATION

Corresponding Author

*E-mail: cle@fct.unl.pt (C.L.), gneves@ua.pt (M.G.P.M.S.N.), ejo14209@fct.unl.pt (E.O.).

Notes

The authors declare no competing financial interest.

■ ACKNOWLEDGMENTS

Authors are grateful to the Scientific PROTEOMASS Association (Portugal) for financial support. Thanks are due to the Fundação para a Ciência e Tecnologia (FCT, Portugal), European Union, QREN, FEDER, and COMPETE for funding the QOPNA research unit (project Pest-C/QUI/UI0062/2011) and the Portuguese National NMR Network, also supported by funds from FCT. C.S., E.O, J.F.B.B, and S.M.S. also thank FCT-MEC (Portugal) for their doctoral and Post-Doctoral grants, SFRH/BD/64155/2009 and SFRH/BPD/72557/2010, SFRH/BPD/63237/2009, and SFRH/BPD/64752/2009, respectively. J.F.L. thanks Scientific PROTEOMASS Association (Portugal) for financial Postdoctoral support.

■ REFERENCES

(1) Lodeiro, C.; Capelo, J. L.; Mejuto, J. C.; Oliveira, E.; Santos, H. M.; Pedras, B.; Nunez, C. *Chem. Soc. Rev.* **2010**, *39*, 2948.

(2) (a) Chen, P.; He, C. *J. Am. Chem. Soc.* **2004**, *126*, 728. (b) Henary, M. M.; Fahrni, C. J. *J. Phys. Chem. A* **2002**, *106*, 5210. (c) Walkup, G. K.; Imperiali, B. *J. Am. Chem. Soc.* **1996**, *118*, 3053.

(3) Aviv-Harel, I.; Gross, Z. *Chem.—Eur. J.* **2009**, *15*, 8382.

(4) Flamigni, L.; Gryko, D. T. *Chem. Soc. Rev.* **2009**, *38*, 1635.

(5) Aviv-Harel, I.; Gross, Z. *Chem. Commun.* **2007**, 1987.

(6) Aviv-Harel, I.; Gross, Z. *Coord. Chem. Rev.* **2011**, *255*, 717.

(7) (a) Ventura, B.; Degli Esposti, A.; Koszarna, B.; Gryko, D. T.; Flamigni, L. *New J. Chem.* **2005**, *29*, 1559. (b) Ding, T.; Aleman, E. A.; Mordarelli, D. A.; Ziegler, C. J. *J. Phys. Chem. A* **2005**, *109*, 7411. (c) Paolesse, R. In *The Porphyrin Handbook*; Kadish, K. M., Smith, K. M., Guilard, R., Eds.; Academic Press: New York, 2000; Vol. *2*, Chapter 11, p 202.

(8) Pariyar, A.; Bose, S.; Chhetri, S. S; Biswas, A. N.; Bandyopadhyay, P. *Dalton Trans.* **2012**, *41*, 3826.

(9) Santos, C. I. M.; Oliveira, E.; Barata, J. F. B.; Faustino, M. A. F.; Cavaleiro, J. A. S.; Neves, M. G. P. M. S.; Lodeiro, C. *J. Mater. Chem.* **2012**, *22*, 13811.

(10) (a) Vale, L.S.H.P; Barata, J. F. B.; Faustino, M. A. F.; Neves, M. G. P. M. S.; Tomé, A. C.; Silva, A. M. S.; Cavaleiro, J. A. S. *Tetrahedron Lett.* **2007**, *48*, 8904. (b) Vale, L. S. H. P.; Barata, J. F. B.; Santos, C. I. M.; Neves, M. G. P. M. S.; Faustino, M. A. F.; Tomé, A. C.; Silva, A. M. S.; Paz, F.A. A; Cavaleiro, J. A.S. *J. Porphyrins Phthalocyanines* **2009**, *13*, 358.

(11) (a) Hussain, S. M.; Hess, K. L.; Gearhart, J. M.; Geiss, K. T.; Schlager, J. J. *Toxicol. In Vitro* **2005**, *19*, 975. (b) Landsdown, A. B. G. *Crit. Rev. Toxicol.* **2007**, *37* (3), 237.

(12) Wygladacz, K.; Radu, A.; Xu, C.; Qin, Y.; Bakker, E. *Anal. Chem.* **2005**, *77*, 4693.

(13) Lione, A. *J. Gen. Pharmacol.* **1985**, *16*, 223.

(14) Crisponi, G.; Nurchi, V. M.; Bertolas, V.; Remelli, M.; Faa, G. *Coord. Chem. Rev.* **2012**, *256*, 89.

(15) (a) Chen, X.; Nam, S.-W.; Jou, M.; Kim, Y.; Kim, S.-J.; Park, S.; Yoon, J. *Org. Lett.* **2008**, *10*, 5235. (b) Nolan, E. M.; Lippard, S. J. *Chem. Rev.* **2008**, *108*, 3443. (c) Tamayo, A.; Pedras, B.; Lodeiro, C.; Escriche, L.; Casabó, J.; Capelo, J. L.; Covelo, B.; Kivekas, R.; Sillampaa, R. *Inorg. Chem.* **2007**, *46*, 7818. (d) Mameli, M.; Lippolis, V.; Caltagirone, C.; Capelo, J. L.; Nieto-Faza, O.; Lodeiro, C. *Inorg. Chem.* **2010**, *49*, 8276.

(16) (a) Rocha, A.; Marques, M. M. B.; Lodeiro, C. *Tetrahedron Lett.* **2009**, *50*, 4930. (b) Swamy, K. M. K.; Kim, H. N.; Soh, J. H.; Kim, Y.; Kim, S.-J.; Yoon, J. *Chem. Commun.* **2009**, 1234. (c) Park, C. S.; Lee, J. Y.; Kang, E.-J.; Lee, J.-E.; Lee, S. S. *Tetrahedron Lett.* **2009**, *50*, 671. (d) Tamayo, A.; Oliveira, E.; Covelo, B.; Casabó, J.; Escriche, Ll.; Lodeiro, C. *Z. Anorg. Allg. Chem.* **2007**, *633*, 1809.

(17) (a) Capelo, J. L.; Maduro, C.; Mota, A. M. *Ultrason. Sonochem.* **2006**, *13*, 98. (b) Nolan, E. M.; Lippard, S. *J. Chem. Rev.* **2008**, *108*, 3443.

(18) Barata, J. F. B.; Daniel-da-Silva, A. L.; Neves, M. G. P. M. S.; Cavaleiro, J. A. S.; Trindade, T. *RSC Adv.* **2013**, *3*, 274.

(19) (a) Berlman, I. B. *Handbook of Fluorescence Spectra of Aromatic Molecules*, 2nd ed.; Academic Press: New York, 1971. (b) Montalti, M.; Credi, A.; Prodi. L.; Gandolfi, M. T. *Handbook of Photochemistry*, 3rd ed.; Taylor & Francis: Boca Raton, FL, 2006.

(20) Sánchez-Iglesias, A.; Pastoriza-Santos, I.; Pérez-Juste, J.; Rodríguez-González, B.; García De Abajo, F.; Liz-Marzán, L. *Adv. Mater.* **2006**, *18*, 2529.

(21) Gryko, D. T.; Koszarna, B. *Org. Biomol. Chem.* **2003**, *2*, 350.

(22) Bendix, J.; Dmochowski, I. J.; Gray, H. B.; Mahammed, A.; Simkhovich, L.; Gross, Z. *Angew. Chem., Int. Ed.* **2000**, *39*, 4048.

(23) Saltsman, I.; Mahammed, A.; Goldberg, I.; Tkachenko, E.; Botoshansky, M.; Gross, Z. *J. Am. Chem. Soc.* **2002**, *124*, 7411.

(24) (a) Ding, T.; Aleman, E. A.; Modarelli, D. A.; Ziegler, C. J. *J. Phys. Chem. A* **2005**, *109*, 7411. (b) Paolesse, R.; Sagnore, F.; Macagnano, A.; Boschi, T.; Prodi, L.; Montalti, M.; Zacchereni, N.; Bolletta, F.; Smith, K. M. *J. Porphyrins Phthalocyanines* **1999**, *3*, 364.

(25) Mahammed, A.; Weaver, J. J.; Gray, H. B.; Abdelas, M.; Gross, Z. *Tetrahedron Lett.* **2003**, *44*, 2077.

(26) Shen, J.; Ou, Z.; Shao, J.; Gałęzowski, M.; Gryko, D. T.; Kadish, K. M. *J. Porphyrins Phthalocyanines* **2007**, *11*, 269.

(27) Jensen, W. B. *J. Chem. Educ.* **2003**, *80* (8), 952.

(28) Gans, P.; Sabatini, A.; Vacca, A. *Talanta.* **1996**, *43*, 1739.

(29) Panzella, L.; Pezzella, A.; Arzillo, M.; Manini, P.; Napolitano, A.; d'Ischia, M. *Tetrahedron.* **2009**, *65*, 2032.

(30) Cotton, F. A; Wilkinson, G. *Advanced Inorganic Chemistry*, 5th ed.; Wiley: New York, 1988; p 735.

(31) Cabbiness, D. K.; Margerum, D. W. *J. Am. Chem. Soc.* **1969**, *91*, 6540.

(32) Theoretical calculations were performed using density-functional theory, with Gaussian09. Molecular geometries were optimized using the unrestricted B3LYP functional with the 6-31G(d,p) basis-set for C, N, F, and H and the ECP LanL2DZ mixed basis set for Ag^{+}, Cu^{2+}, and Al^{3+}.

(33) Frisch, M. J.; Trucks, G. W.; Schlegel, H. B.; Scuseria, G. E.; Robb, M. A.; Cheeseman, J. R.; Scalmani, G.; Barone, V.; Mennucci, B.; Petersson, G. A.; Nakatsuji, H.; Caricato, M.; Li, X.; Hratchian, H. P.; Izmaylov, A. F.; Bloino, J.; Zheng, G.; Sonnenberg, J. L.; Hada, M.; Ehara, M.; Toyota, K.; Fukuda, R.; Hasegawa, J.; Ishida, M.; Nakajima, T.; Honda, Y.; Kitao, O.; Nakai, H.; Vreven, T.; Montgomery Jr., J. A.; Peralta, J. E.; Ogliaro, F.; Bearpark, M.; Heyd, J. J.; Brothers, E.; Kudin, K. N.; Staroverov, V. N.; Kobayashi, R.; Normand, J.; Raghavachari, K.; Rendell, A.; Burant, J. C.; Iyengar, S. S.; Tomasi, J.; Cossi, M.; Rega, N.; Millam, J. M.; Klene, M.; Knox, J. E.; Cross, J. B.; Bakken, V.; Adamo, C.; Jaramillo, J.; Gomperts, R.; Stratmann, R. E.; Yazyev, O.; Austin, A. J.; Cammi, R.; Pomelli, C.; Ochterski, J. W.; Martin, R. L.; Morokuma, K.; Zakrzewski, V. G.; Voth, G. A.; Salvador, P.; Dannenberg, J. J.; Dapprich, S.; Daniels, A. D.; Farkas, Ö.; Foresman, J. B.; Ortiz, J. V.; Cioslowski, J.; Fox, D. J. *Gaussian 09*, Revision A.02; Gaussian, Inc.: Wallingford, CT, 2009.

(34) Cotton, F. A; Wilkinson, G.; Murillo, C. A. *Advanced Inorganic Chemistry*, 6th ed.; Wiley: New York, 1999.